

Diffuse-interface lattice Boltzmann modeling of charged particle transport in Poiseuille flowJiao Liu,¹ Zhenhua Chai^{1,2,3,*} and Baochang Shi^{1,2,3}¹*School of Mathematics and Statistics, Huazhong University of Science and Technology, Wuhan 430074, China*²*Institute of Interdisciplinary Research for Mathematics and Applied Science, Huazhong University of Science and Technology, Wuhan 430074, China*³*Hubei Key Laboratory of Engineering Modeling and Scientific Computing, Huazhong University of Science and Technology, Wuhan 430074, China*

(Received 27 January 2022; revised 11 June 2022; accepted 24 June 2022; published 18 July 2022)

In this paper, we developed a coupled diffuse-interface lattice Boltzmann method (DI-LBM) to study the transport of a charged particle in the Poiseuille flow, which is governed by the Navier-Stokes equations for fluid field and the Poisson-Boltzmann equation for electric potential field. We first validated the present DI-LBM through some classical benchmark problems, and then investigated the effect of electric field on the lateral migration of the particle in the Poiseuille flow. The numerical results show that the electric field has a significant influence on the particle migration. When an electric field in the vertical direction is applied to the charged particle initially located above the centerline of the channel, the equilibrium position of the particle would drop suddenly as the electric field is larger than a critical value. This is caused by the wall repulsion due to lubrication, the inertial lift related to shear slip, the lift owing to particle rotation, the lift due to the curvature of the undisturbed velocity profile, and the electric force. On the other hand, when an electric field in the horizontal direction is adopted, the equilibrium position of the particle would move toward the centerline of the channel with the increase of the electric field.

DOI: [10.1103/PhysRevE.106.015306](https://doi.org/10.1103/PhysRevE.106.015306)**I. INTRODUCTION**

The transport of a particle in the Poiseuille flow, as a basic prototype of particulate flows, has received increasing attention for its significance in a variety of industrial and biological applications [1–3]. Segre and Silberberg [1] first conducted an experimental study on the neutrally buoyant particle in the Poiseuille flow and found that the particle always migrates to the equilibrium position between the centerline and the wall, which is the so-called Segre-Silberberg phenomenon, and is also investigated theoretically in the later works. For example, Cox and Brenner [4] considered a spherical particle suspended in a three-dimensional Poiseuille flow, and derived a theoretical expression of the migration velocity. Ho and Leal [5] theoretically investigated the motion of a neutrally buoyant particle in a two-dimensional Couette and Poiseuille flow, and found that the particle reached a stable lateral equilibrium position independent of the initial position of release. Then Vasseur and Cox [6] studied the migration of neutral and non-neutral buoyant particles in the Couette and Poiseuille flows with the method developed in Ref. [4].

On the other hand, with the development of computational techniques, the numerical simulation, as a more popular approach, has also been used to study the dynamic behavior of the particle in the Poiseuille flow. For instance, Feng *et al.* [7] studied the motion of a circular particle in the Poiseuille flow with the finite-element method (FEM). They reported the mechanisms of a circular particle in the Poiseuille flow,

and found that their results are qualitatively consistent with the available data. Inamuro *et al.* [8] investigated the motion of one and two lines of neutrally buoyant circular cylinders between flat parallel walls by the lattice Boltzmann method (LBM), and also observed the Segre-Silberberg phenomenon for both a single and two lines of cylinders. Shao *et al.* [9] considered the inertial migration of spherical particles in the Poiseuille flow by using a fictitious domain method, and found that the results are in a qualitative agreement with the theoretical and experimental data. Hu *et al.* [10] studied the influence of thermal convection on a neutrally buoyant particle migration in the Poiseuille flow via the LBM, and illustrated that when the Grashof number exceeds a critical value, the equilibrium position of the particle would change from the upper part to the lower part of the channel.

It should be noted that most of these previous studies focused on the uncharged particle migration in the Poiseuille flow. In reality, however, the particle could be charged, and the electrostatic force would have a significant effect on the particle migration. Actually, the transport of the charged particle also attained great interest in the past years. Ye *et al.* [11] investigated the electrophoretic motion of two spherical particles in an aqueous electrolyte solution by the FEM, and found that the faster particle, moving behind the slower particle, would climb and pass the slower particle when the two particles' centers are not located on the same line parallel to the applied electric field. Bhattacharyya *et al.* [12] focused on the migration of a colloidal particle in an electrolyte solution under the influence of an external electric field. It is demonstrated that as the particle velocity rises, the hydrodynamic drag gradually approaches the Stokes drag and the

*Corresponding author: hustczh@hust.edu.cn

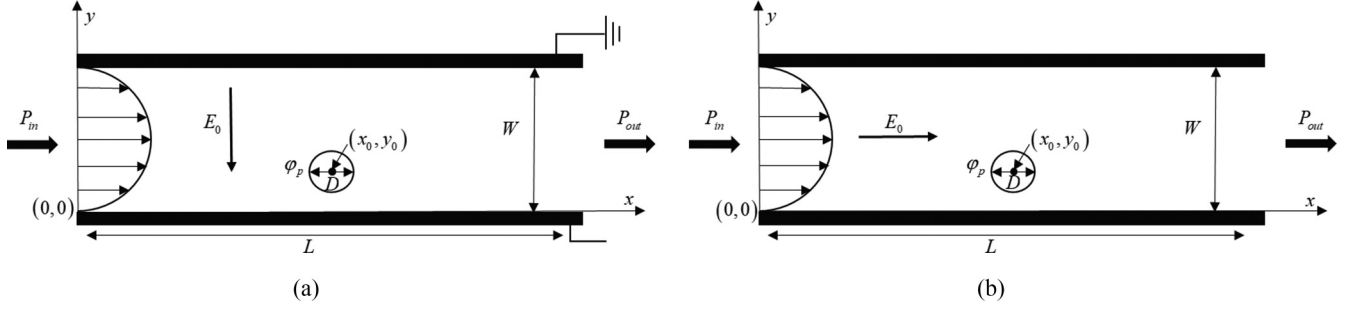


FIG. 1. Schematic of the physical problem [(a) an electric field applied in vertical direction, (b) an electric field applied in horizontal direction].

electric force diminishes. Xie *et al.* [13] considered the two-dimensional interactive motion of multiple dielectrophoretic particles in an electrolyte subjected to a uniform DC electric field, and found that the behavior of interactive motion of dielectrophoretic particles is affected significantly by the difference of permittivity between the particle and electrolyte. Tofighi *et al.* [14] investigated the sedimentation of an elliptic disk under an electrostatic field by using the smooth particle hydrodynamics method, and showed that for the specified blockage and density ratios, the final sedimentation orientation of the ellipse disk is dependent on the electric field intensity. To our knowledge, the particle in the Poiseuille flow, as a classic problem, has been studied extensively; however, a charged particle in the Poiseuille flow under the influence of an external electric field has not been considered. In this work, we will study the migration of a charged particle in the Poiseuille flow with the LBM, and focus on the influence of an external electric field.

The lattice Boltzmann method, as a kinetic-based numerical approach, has gained great success in the study of complex hydrodynamic problems [15–20]. Compared to the traditional numerical methods, the LBM has some distinct advantages, including the clear physical background, easy implementation of complex boundary conditions, natural parallelism in algorithm, and simplicity in programming [15]. Due to these advantages of the LBM, it has also been applied to investigate particulate flows [21–23]. Recently, an efficient approach, named the diffuse-interface LBM (DI-LBM) [24], is developed for the fluid-particle interaction problems. In this method, the fluid is filled with the whole domain, and the sharp boundary between the fluid and particle is replaced by a diffuse interface with a nonzero thickness, in which the physical variables are assumed to change smoothly. In addition, the fluid-particle interaction is realized through modifying the force term in the evolution equation, and there is no special treatment on the fresh fluid nodes. Owing to the advantages of the DI-LBM in the study of fluid-particle problems, it will be extended to study the problem of a charged particle in the Poiseuille flow.

The rest of the paper is organized as follows. In Sec. II, the physical problem and macroscopic governing equations are briefly introduced. In Sec. III, a triple-distribution-function DI-LBM for the governing equations is developed, followed by the numerical validations in Sec. IV. In Sec. V, the electric field effect on the lateral migration of the particle in

the Poiseuille flow is mainly investigated, and finally some conclusions are given in Sec. VI.

II. PHYSICAL PROBLEM AND MACROSCOPIC GOVERNING EQUATIONS

The schematic of the physical problem we consider is shown in Fig. 1, where a neutrally buoyant particle with the diameter $D = 1$ (unless otherwise stated) is placed in a channel with $L \times W = 20D \times 4D$. The initial position of the particle is located at (x_0, y_0) with $x_0 = L/2$. The electric potential of the particle surface is φ_p , and a uniform external electrical field E_0 is applied in the vertical (negative y) direction and the horizontal (positive x) direction, respectively. The pressure drop from inlet to outlet is $\Delta P = P_{in} - P_{out}$, and the no-slip boundary conditions are applied to the channel walls.

For the above physical problem, the governing equations, including the Navier-Stokes equations, the internal electric potential equation, and the external electric potential equation, can be expressed as

$$\nabla \cdot \mathbf{u} = 0, \quad (1)$$

$$\rho \left(\frac{\partial \mathbf{u}}{\partial t} + \mathbf{u} \cdot \nabla \mathbf{u} \right) = -\nabla P + \nabla \cdot (\mu \nabla \mathbf{u}) + \mathbf{F}, \quad (2)$$

$$\nabla^2 \varphi = -\frac{\rho_e}{\varepsilon \varepsilon_0}, \quad (3)$$

$$\nabla^2 \psi = 0, \quad (4)$$

where ρ , \mathbf{u} , and P are the fluid density, velocity, and pressure and μ is the dynamic viscosity. The parameters ψ , φ , ε , and ε_0 denote the external electric potential, internal electric potential, dimensionless dielectric constant, and permittivity of vacuum. The external force \mathbf{F} is given by $\mathbf{F} = \rho_e \mathbf{E}$ where $\rho_e = -2n_\infty z e \sinh(\frac{ze\varphi}{k_b T})$ is the net charge density, n_∞ is the ionic number concentration in the bulk solution, z is the valence of ions, e is the fundamental electric charge, k_b is the Boltzmann constant, T is the temperature, and $\mathbf{E} = -(\nabla \psi + \nabla \varphi)$ is the total electric field. The boundary condition of the external electric potential at particle surface is $\nabla_n \psi = 0$.

It is known that when the surface electric potential is small enough, the Debye-Hückel approximation ($\sinh(\frac{ze\varphi}{k_b T}) \approx \frac{ze\varphi}{k_b T}$) can be applied, and Eq. (3) can be simplified by

$$\nabla^2 \varphi = \frac{2n_\infty z^2 e^2}{\varepsilon \varepsilon_0 k_b T} \varphi = \kappa^2 \varphi, \quad (5)$$

where $\kappa = \sqrt{\frac{2n_\infty z^2 e^2}{\varepsilon \varepsilon_0 K_b T}}$ is the reciprocal of the Debye length.

To simplify the following analysis, we introduce some dimensionless variables,

$$\begin{aligned} x^* &= \frac{x}{d_0}, & u^* &= \frac{u}{u_0}, & t^* &= \frac{t}{d_0/u_0}, & \rho^* &= \frac{\rho}{\rho_0}, \\ P^* &= \frac{P}{\rho_0 u_0^2 / d_0}, & \varphi^* &= \frac{\varphi}{\varphi_0}, \end{aligned} \quad (6)$$

which can be used to derive the dimensionless governing equations,

$$\nabla \cdot \mathbf{u} = 0, \quad (7)$$

$$\rho \frac{\partial \mathbf{u}}{\partial t} + \rho \mathbf{u} \cdot \nabla \mathbf{u} = -\nabla P + \nabla \cdot \left(\frac{1}{Re} \nabla \mathbf{u} \right) + \bar{\rho}_e \mathbf{E}, \quad (8)$$

$$\nabla^2 \varphi = \lambda^2 \varphi, \quad (9)$$

$$\nabla^2 \psi = 0, \quad (10)$$

where the superscript $*$ has been omitted. The dimensionless parameters Re , $\bar{\rho}_e$, and λ are defined as

$$Re = \frac{u_0 d_0 \rho_0}{\mu}, \quad \bar{\rho}_e = -\frac{\kappa^2 \varepsilon \varepsilon_0 \varphi_0^2}{\rho_0 u_0^2} \varphi, \quad \lambda = \kappa d_0. \quad (11)$$

Besides the above governing equations for fluid and electric fields, we also need to consider the following equations for the motion of the particle,

$$m_p \frac{d\mathbf{u}_p}{dt} = \mathbf{F}_h + \mathbf{F}_e + \left(\frac{\rho}{\rho_p} - 1 \right) m_p \mathbf{g}, \quad (12)$$

$$I_p \frac{d\omega_p}{dt} = T_h + T_e, \quad (13)$$

$$\frac{d\mathbf{x}_p}{dt} = \mathbf{u}_p, \quad (14)$$

where m_p and I_p are the mass and rotational inertia of the particle, ρ_p and \mathbf{u}_p are the particle density and translational velocity, ω_p is the angular velocity of the particle, and \mathbf{g} is the gravity acceleration. \mathbf{x}_p is the position of the particle, and \mathbf{F}_h and \mathbf{F}_e are the hydrodynamic and electrostatic forces. T_h and T_e are hydrodynamic and electrostatic torques.

III. NUMERICAL METHOD

A. The diffuse-interface lattice Boltzmann method

To depict the transport of a charged particle in the Poiseuille flow, a triple-distribution-function DI-LBM is developed. In this method, the evolution equations for fluid field and internal and external electric fields are written as

$$\begin{aligned} f_i(\mathbf{x} + \mathbf{c}_i \Delta t, t + \Delta t) &= f_i(\mathbf{x}, t) - \frac{1}{\tau_f} [f_i(\mathbf{x}, t) - f_i^{\text{eq}}(\mathbf{x}, t)] \\ &+ \Delta t (1 - \phi) F_i(\mathbf{x}, t) + \bar{F}_i(\mathbf{x}, t), \end{aligned} \quad (15)$$

$$\begin{aligned} g_i(\mathbf{x} + \mathbf{c}_i \Delta t, t + \Delta t) &= g_i(\mathbf{x}, t) - \frac{1}{\tau_g} [g_i(\mathbf{x}, t) - g_i^{\text{eq}}(\mathbf{x}, t)] \\ &+ \Delta t (1 - \phi) \alpha G_i(\mathbf{x}, t) + \Delta t \phi \alpha \bar{G}_i(\mathbf{x}, t), \end{aligned} \quad (16)$$

$$\begin{aligned} h_i(\mathbf{x} + \mathbf{c}_i \Delta t, t + \Delta t) &= h_i(\mathbf{x}, t) - \frac{1}{\tau_h} [h_i(\mathbf{x}, t) - h_i^{\text{eq}}(\mathbf{x}, t)] + \Delta t \phi \alpha H_i(\mathbf{x}, t), \end{aligned} \quad (17)$$

where Δt and Δx are the time step and lattice spacing, and τ_f , τ_g , and τ_h are the relaxation times for the flow and internal and external electric potential fields. α is an artificial diffusion coefficient [25,26]. $\mathbf{c}_i = c \mathbf{e}_i$ is the discrete velocity vector with $c = \Delta x / \Delta t$ being the lattice speed. The equilibrium distribution functions $f_i^{\text{eq}}(\mathbf{x}, t)$, $g_i^{\text{eq}}(\mathbf{x}, t)$, and $h_i^{\text{eq}}(\mathbf{x}, t)$ are defined as [17,25,26]

$$f_i^{\text{eq}}(\mathbf{x}, t) = \rho w_i \left(1 + \frac{\mathbf{c}_i \cdot \mathbf{u}}{c_s^2} + \frac{(\mathbf{c}_i \cdot \mathbf{u})^2}{2c_s^4} - \frac{\mathbf{u}^2}{2c_s^2} \right), \quad (18)$$

$$g_i^{(\text{eq})}(\mathbf{x}, t) = \begin{cases} (w'_0 - 1)\varphi, & i = 0, \\ w'_i \varphi, & i \neq 0, \end{cases} \quad (19)$$

$$h_i^{(\text{eq})}(\mathbf{x}, t) = \begin{cases} (w'_0 - 1)\psi, & i = 0, \\ w'_i \psi, & i \neq 0, \end{cases} \quad (20)$$

where w_i and w'_i are the weight coefficients. c_s is the lattice sound speed and is related to lattice speed c . To make the model more efficient, the popular D2Q9 and D2Q5 lattice models [27] are considered for the flow and electric potential fields, respectively. In the D2Q9 model, $w_0 = 4/9$, $w_{1-4} = 1/9$, $w_{5-8} = 1/36$, and $c_s^2 = c^2/3$, while in the D2Q5 model, $w'_0 = 0$, $w'_{1-4} = 1/4$, and $c_s^2 = c^2/2$.

The parameter ϕ is a hyperbolic tangent function and is defined as

$$\phi = \frac{1 + \tanh(2l/\varepsilon_d)}{2}, \quad (21)$$

where l is the distance of the node to the boundary of the particle, and ε_d is the thickness of diffuse interface. F_i and G_i are the discrete force and source terms, and can be given by [28]

$$F_i = w_i \left(1 - \frac{1}{2\tau_f} \right) \left(\frac{\mathbf{c}_i - \mathbf{u}}{c_s^2} + \frac{\mathbf{c}_i \cdot \mathbf{u}}{c_s^4} \mathbf{c}_i \right) \cdot \bar{\rho}_e \mathbf{E}, \quad (22)$$

$$G_i = w'_i \lambda^2 \varphi. \quad (23)$$

In addition, to describe the fluid-particle interaction properly, the terms \bar{F}_i , \bar{G}_i , and H_i are adopted, and they should be given by

$$\begin{aligned} \bar{F}_i &= \phi \left(1 - \frac{1}{2\tau_f} \right) w_i \rho \left(\frac{\mathbf{c}_i \cdot (\mathbf{u}_s - \mathbf{u}^*)}{c_s^2} \right. \\ &\left. + \frac{(\mathbf{u}_s \cdot \mathbf{u}_s - \mathbf{u}^* \cdot \mathbf{u}^*) : (\mathbf{c}_i \mathbf{c}_i - c_s^2 \mathbf{I})}{2c_s^4} \right), \end{aligned} \quad (24)$$

$$\bar{G}_i = w'_i \frac{(\varphi_p - \varphi)}{\Delta t}, \quad (25)$$

$$H_i = w'_i \frac{(-\nabla_n \psi)}{\Delta x}, \quad (26)$$

where φ_p denotes the surface potential of the particle, and \mathbf{u}_s is the velocity of the particle ($\mathbf{u}_s = \mathbf{u}_p + \omega_p \times (\mathbf{x} - \mathbf{x}_p)$); \mathbf{x} is the coordinate of the grid). \mathbf{u}^* is the velocity without considering

the fluid-particle interaction, and it is calculated by

$$\mathbf{u}^* = \frac{\sum_i \mathbf{c}_i f_i + \frac{\Delta t(1-\phi)}{2} \bar{\rho}_e \mathbf{E}}{\rho}. \quad (27)$$

Through considering the interaction between the particle and fluid, the macroscopic quantities can be determined by

$$\rho = \sum_i f_i, \quad (28)$$

$$\mathbf{u} = \mathbf{u}^* + \frac{1}{2} \phi (\mathbf{u}_s - \mathbf{u}^*), \quad (29)$$

$$\varphi = \frac{\sum_{i=1}^{q-1} g_i + w'_0(1-\phi)\tau_g \Delta t \alpha G + w'_0 \phi \tau_g \alpha \varphi_p}{1 - w'_0 + w'_0 \phi \tau_g \alpha}, \quad (30)$$

$$\psi = \frac{1}{1 - w'_0} \sum_{i=1}^{q-1} h_i - \frac{w'_0}{1 - w'_0} \phi \tau_h \Delta t \alpha \nabla_n \psi / \Delta x. \quad (31)$$

Finally, through the Chapman-Enskog analysis [17], the governing equations can be recovered with the following viscosity and artificial diffusion coefficient,

$$\mu = \rho_0 c_s^2 \left(\tau_f - \frac{1}{2} \right) \Delta t, \quad (32)$$

$$\alpha = c_s^2 \left(\frac{1}{2} - \tau_g \right) \Delta t = c_s^2 \left(\frac{1}{2} - \tau_h \right) \Delta t. \quad (33)$$

Due to the kinetic nature of the LBM, the gradient terms $\nabla \varphi$ and $\nabla \psi$ can be calculated by the following second-order local schemes [25,26],

$$\nabla \varphi = -\frac{1}{\tau_g \Delta t c_s^2} \sum_i \mathbf{c}_i g_i, \quad (34)$$

$$\nabla \psi = -\frac{1}{\tau_h \Delta t c_s^2} \sum_i \mathbf{c}_i h_i. \quad (35)$$

B. Numerical approach for particle movement

Here for simplicity, we adopt the first-order Euler method for Eqs. (12), (13), and (14),

$$\mathbf{u}_p^{n+1} = \mathbf{u}_p^n + \frac{\Delta t}{m_p} \left[\mathbf{F}_h + \mathbf{F}_e + \left(\frac{\rho}{\rho_p} - 1 \right) m_p \mathbf{g} \right], \quad (36)$$

$$\omega_p^{n+1} = \omega_p^n + \frac{\Delta t}{I_p} (T_h + T_e), \quad (37)$$

$$\mathbf{x}_p^{n+1} = \mathbf{x}_p^n + \Delta t \mathbf{u}_p. \quad (38)$$

In the implementation of Eq. (36) for the motion of the charged particle, the electrostatic force \mathbf{F}_e and hydrodynamic force \mathbf{F}_h acting on the particle have to be determined beforehand. In the framework of LBM, the hydrodynamic force \mathbf{F}_h and torque T_h can be calculated by

$$\mathbf{F}_h = -\frac{\Delta x^2}{\Delta t} \sum_n \phi_n \rho (\mathbf{u}_s - \mathbf{u}^*), \quad (39)$$

$$T_h = -\frac{\Delta x^2}{\Delta t} \sum_n (\mathbf{x}_n - \mathbf{x}_p) \times [\phi_n \rho (\mathbf{u}_s - \mathbf{u}^*)], \quad (40)$$

where \mathbf{x}_n is the coordinate of the node n . The electrostatic force \mathbf{F}_e and torque T_e are computed by

$$\mathbf{F}_e = \sum_{\partial \Gamma} \sigma_e \cdot \mathbf{n} \Delta s, \quad (41)$$

$$T_e = \sum_{\partial \Gamma} (\mathbf{x} - \mathbf{x}_p) \times \sigma_e \cdot \mathbf{n} \Delta s, \quad (42)$$

where $\sigma_e = \frac{\varepsilon \varepsilon_0 \phi_0^2}{\rho_0 u_0^2 d_0^2} (\mathbf{E}\mathbf{E} - 1/2 |\mathbf{E}|^2 \mathbf{I})$ is the Maxwell stress tensor, \mathbf{n} is the outward unit vector normal to the interface of the particle, and Δs is the unit arc length of the particle surface.

IV. NUMERICAL VALIDATIONS

In this section, three benchmark problems are used to test the accuracy of the present DI-LBM. The first one is the inertial migration of an uncharged neutral buoyant particle in the Poiseuille flow, the second one is a particle with a uniform surface charge immersed in an electrolyte solution, and the third one is the coaxial electrophoretic motion of a spherical particle.

A. An uncharged neutral buoyant particle moving in the Poiseuille flow

The configuration of this problem is similar to that in Fig. 1, and the only difference is that the electric field is not included. The pressure drop from inlet to outlet is set to be $\Delta P = 0.00267$, the lattice spacing is $\Delta x = 1/25$, and the relaxation time is $\tau_f = 0.75$. The channel Reynolds number is $\text{Re} = 96.12$, and the particle is released at initial position $(x_0, y_0) = (L/2, 0.25W)$.

Figure 2 shows the trajectory of the particle, and a comparison of the results of Tao *et al.* [29] and the homogenized lattice Boltzmann method (HLBM) [30] is also made. From this figure, one can observe that with the increase of time, the particle would finally reach the equilibrium position between the wall and the centerline of the channel ($y = 0.5W$), which is in good agreement with the data reported in Ref. [29] and obtained by HLBM. In addition, to give a quantitative comparison, we also measured the equilibrium position of the particle, and presented the results of different methods in Table I. As seen from this table, our result is very close to those of Ref. [29] and HLBM.

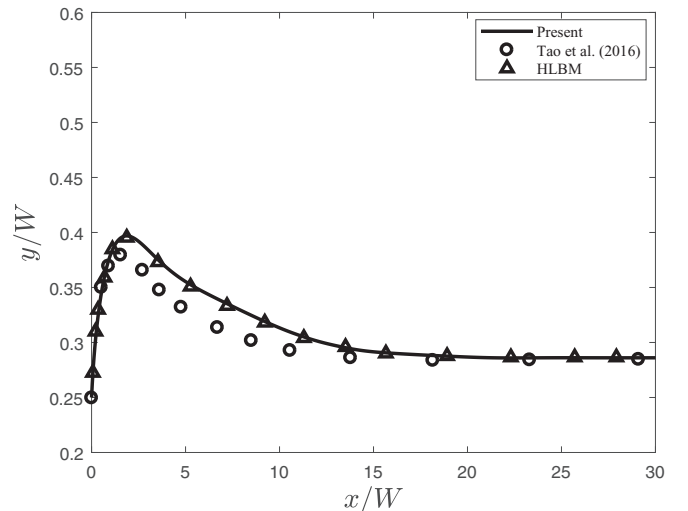


FIG. 2. The trajectory of the moving particle in the Poiseuille flow.

TABLE I. A comparison of the particle equilibrium position between the present work and some previous studies.

Present	Tao <i>et al.</i> [29]	HLBM
0.2861	0.2849	0.2872

B. A particle with a uniform surface charge immersed in an electrolyte solution

To further test the capacity of the DI-LBM in describing the distribution of electric potential around the charged particle, the problem of a particle with a uniform surface charge immersed in an electrolyte solution is considered. As shown in Fig. 3, the computational domain is $Lx \times Ly = 30 \times 30$, and the particle with the diameter $D = 1.0$ is fixed at the center of the domain. The dimensionless parameter $\lambda = 10$, and the electric potential on the particle surface is set as $\varphi_p = 1.0$. Under the no-flux boundary condition applied for all the physical variables, one can obtain the following analytical solution,

$$\varphi = \frac{\varphi_p B_2(\lambda r)}{B_2(\lambda D/2)}, \quad r \geq D/2, \quad (43)$$

where B_2 is the second kind of Bessel function and r is the distance to the center of the particle.

We performed a simulation with the lattice spacing $\Delta x = 1/25$ and the relaxation time $\tau_g = 0.75$, and presented a comparison of analytical and numerical solutions along the horizontal centerline in Fig. 4. From this figure, one can see that the numerical solution agrees well with the analytical solution.

C. The coaxial electrophoretic motion of a spherical particle

The last validation problem we considered is the coaxial electrophoretic motion of a spherical particle with the radius a in a long cylindrical tube with the radius b . The parameter $\kappa a \approx 1$, the electric potentials on the particle surface and cylindrical tube surface are $\varphi_p = 1.0$ mV and $\varphi_m = 0.0$ mV, and the other parameters are the same as those in Ref. [31]. We performed some simulations with the D3Q15 lattice model, and presented the velocity of the spherical particle as a

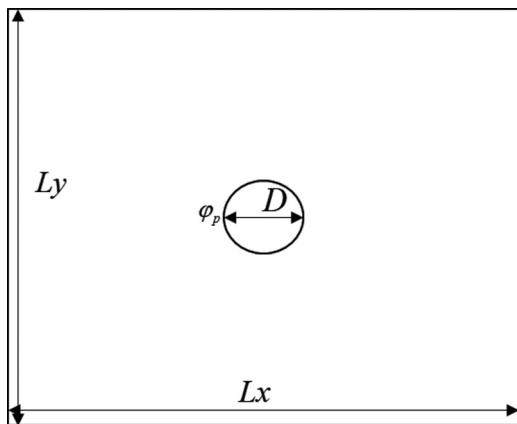


FIG. 3. Schematic of a charged particle immersed in an electrolyte solution.

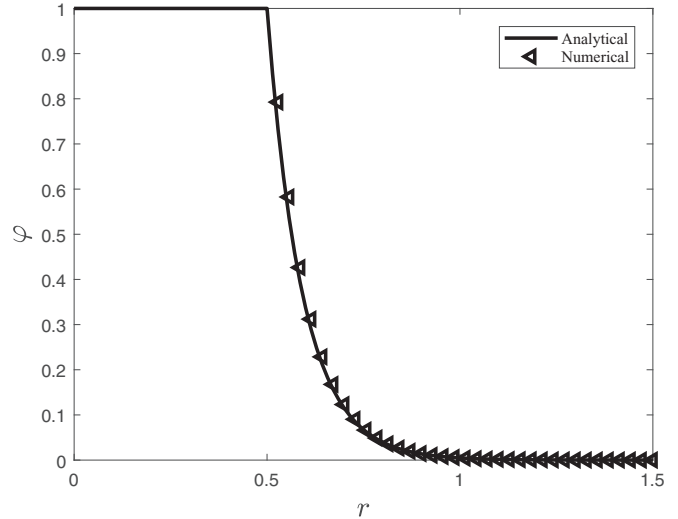


FIG. 4. Analytical and numerical solutions of the electric potential around the circular particle with a uniform surface charge.

function of the radius ratio a/b in Fig. 5 where the velocity of the particle is normalized with $U_{eq} = \epsilon\epsilon_0\varphi_p E/\mu$. As shown in this figure, the velocity of the particle decreases with the increase of a/b , which is in good agreement with the available data [31].

V. NUMERICAL RESULTS AND DISCUSSION

In this section, we will perform some simulations to study the lateral migration of a charged neutral buoyant particle in the Poiseuille flow under an external electric field. To this end, a grid-independent test is first conducted under different lattice sizes, and then the particle migration under the vertical and horizontal electric fields is investigated.

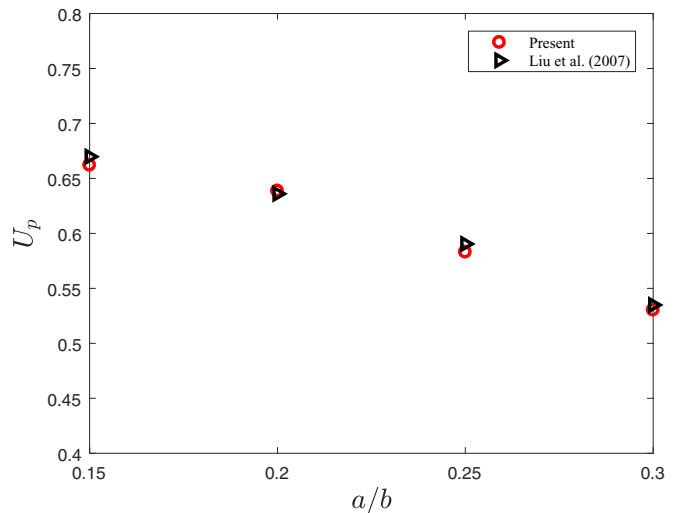


FIG. 5. The velocity U_p of the spherical particle against the radius ratio a/b .

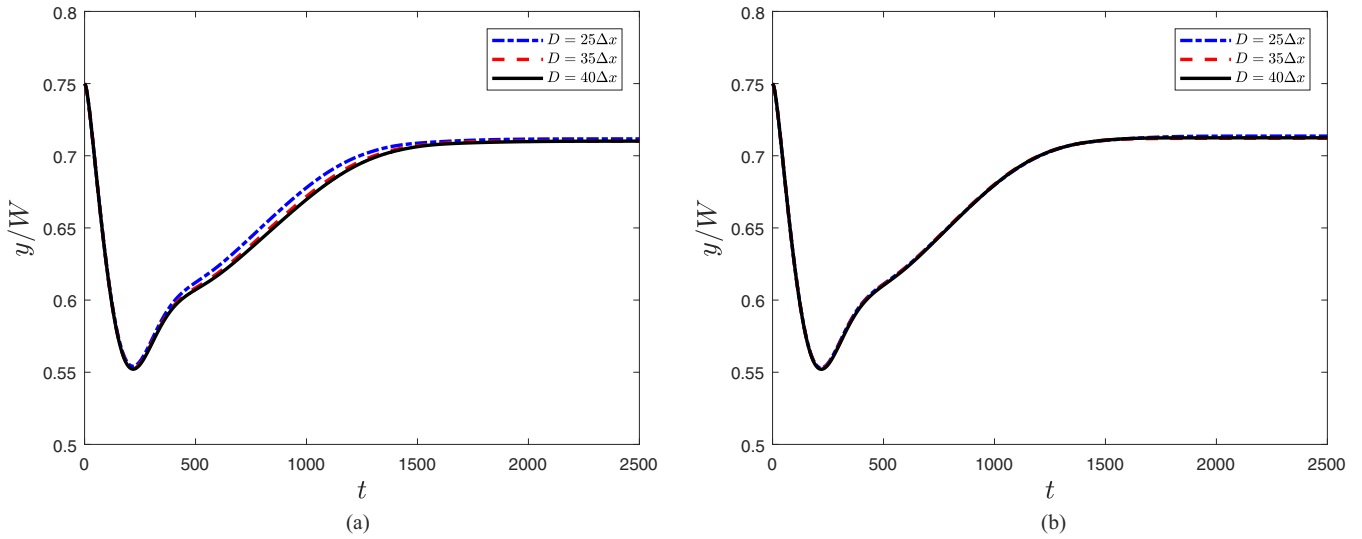


FIG. 6. The lateral positions of the particle at different D lattice resolutions and time [(a) the case with a vertical electric field, (b) the case with a horizontal electric field].

A. A grid-independent test

A grid-independent test on the physical problem shown in Fig. 1 is first carried out under different lattice resolutions. The pressure difference is set to be $\Delta P = 0.00267$, the corresponding channel Reynolds number is $Re = 96.12$, and the other parameters are $\lambda = 10$ and $\bar{\rho}_e = -6.95 \times 10^{-5}\varphi$. The initial position of the particle is fixed at $y_0 = 0.75W$, and the external electric field is $E_0 = 1$. The electric potential on the particle surface is $\phi_p = 1.0$ for the case with a vertical external electric field and $\phi_p = -1.0$ for the case with a horizontal external electric field. Figure 6 shows the lateral trajectories of the particle under different grid resolutions. It can be found from this figure that the results under $D = 35\Delta x$ and $D = 40\Delta x$ are almost the same as each other, and for this reason, the grid resolution $D = 35\Delta x$ is adopted in the following simulations.

B. The charged particle motion under a vertical external electric field

We now performed some simulations to study the effect of the vertical external electric field on the lateral migration of the charged particle, and focused on three cases with the initial positions $y_0 = 0.75W$, $0.65W$, and $0.25W$. We conducted some simulations under different values of the external electric field intensity E_0 , and presented the lateral equilibrium position y_{eq} of the charged particle in Fig. 7. Based on the results shown in this figure, one can observe that for the cases with $y_0 = 0.75W$ and $0.65W$, the equilibrium position is still above the centerline as electric field density E_0 is small enough, while it would gradually approach the centerline with the increase of E_0 . In particular, when E_0 is larger than a critical value E_c , the equilibrium position of the case with $y_0 = 0.75W$ would reduce suddenly from $0.69W$ above the

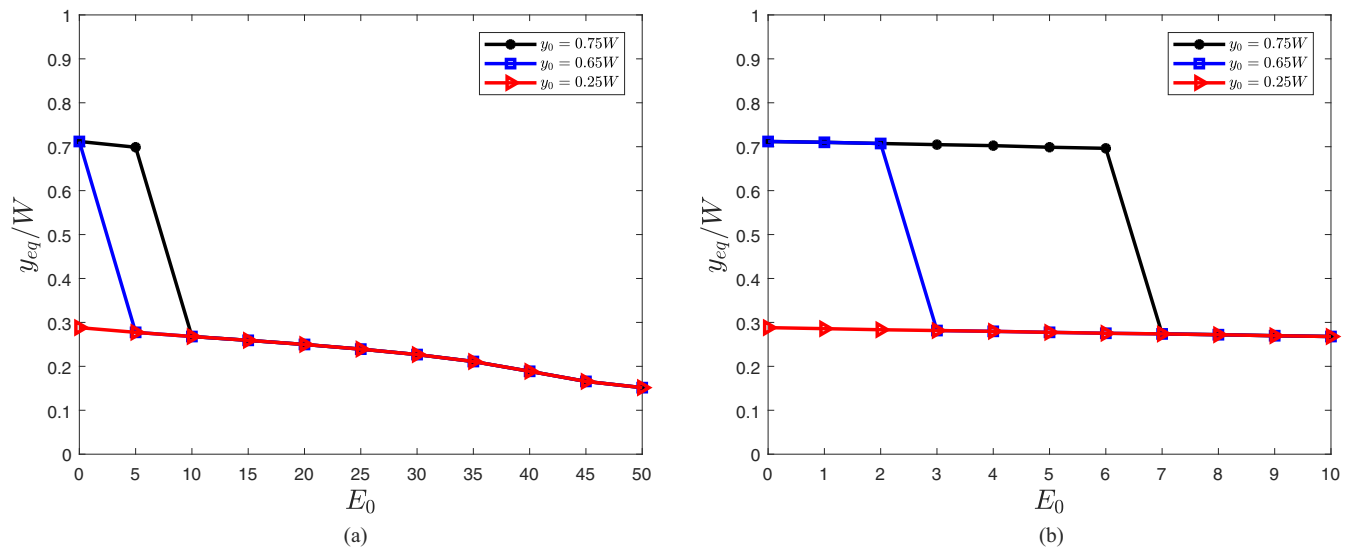


FIG. 7. The effect of vertical electric field on the lateral equilibrium position y_{eq} of the particle: (a) $E_0 \in [0, 50]$, (b) $E_0 \in [0, 10]$.

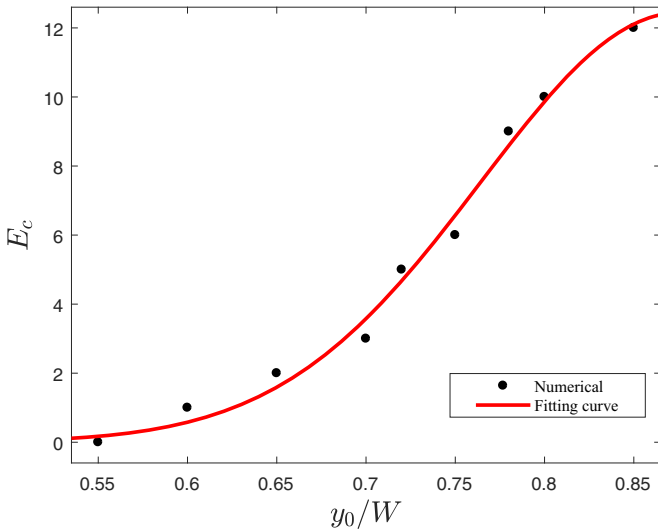


FIG. 8. The relation between the critical electric field intensity E_c and the initial position y_0 .

centerline to $0.27W$ below the centerline. For the case with $y_0 = 0.25W$, however, the equilibrium position is below the centerline and gradually approaches the wall with the increase of E_0 . It should also be noted that the equilibrium position of the charged particle is related to the initial position for a small E_0 , but it would be independent on the initial position as E_0 is large enough. In addition, from Fig. 7(b) one can also find that for the cases with $y_0 = 0.65W$ and $0.75W$, the critical values of electric field density E_0 are about 2 and 6, which means that as E_0 increases, the initial position is closer to the centerline and the transition of the equilibrium position is earlier. To see this more clearly, we presented the values of critical electric field intensity (E_c) with different initial positions (y_0) in Fig. 8, and a least-square fitting gives the following approximate expression,

$$E_c = 12.44 \exp \left[- \left(\frac{y_0/W - 0.8758}{0.1576} \right)^2 \right], \quad y_0 > 0.5W, \quad (44)$$

which shows that E_c increases exponentially with y_0 . We also gave a special discussion on the critical value of electric field intensity E_c for the case with $y_0 = 0.75W$. In order to explore the interesting bifurcation phenomenon, we presented the time evolutions of the particle lateral position at $E_0 = 6$ and $E_0 = 7$ in Fig. 9. When the dimensionless time $t\nu/D^2$ ($\nu = \mu/\rho$ denotes the kinematic viscosity) is no more than 1.4, the particle trajectories are almost the same for both cases of $E_0 = 6$ and 7, and the bifurcation phenomenon begins to occur after $t\nu/D^2 = 1.4$. Particularly, for case of $E_0 = 6$, the particle rises and reaches its equilibrium position above the centerline, while for $E_0 = 7$, the particle would descend and cross the centerline to reach an equilibrium position below the centerline.

We also tested the effect of the particle size on the equilibrium position, and plotted the results in Fig. 10, where the initial position of the charged particle is $y_0 = 0.75W$. As seen from this figure, the critical value for the transition of particle equilibrium position is different for different particle

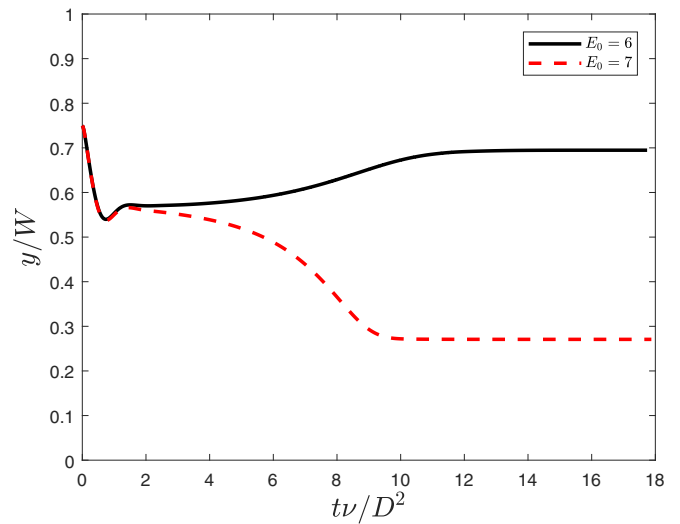


FIG. 9. Time evolutions of the lateral position of the particle at $E_0 = 6$ and $E_0 = 7$.

sizes. With the increase of E_0 , the smaller particle has a earlier transition of the equilibrium position.

We now try to understand the phenomena observed above from a mechanical point of view. It is known that for the uncharged neutrally buoyant particle in the Poiseuille flow, the lateral equilibrium position is determined by four different mechanisms [7], i.e., the wall repulsion due to lubrication, the inertial lift related to shear slip, the two lifts due to particle rotation, and the curvature of the undisturbed velocity profile. As the electric field is involved, however, another mechanism related to the electric force should be considered. Actually, when a vertical electric field with a negative value is applied, the particle experiences a downward force and moves toward the wall. In the following, a detailed analysis on the above mechanisms is performed to explain the interesting bifurcation phenomenon. First of all, the effect of the wall is to force the particle away from the wall to the center of the channel,

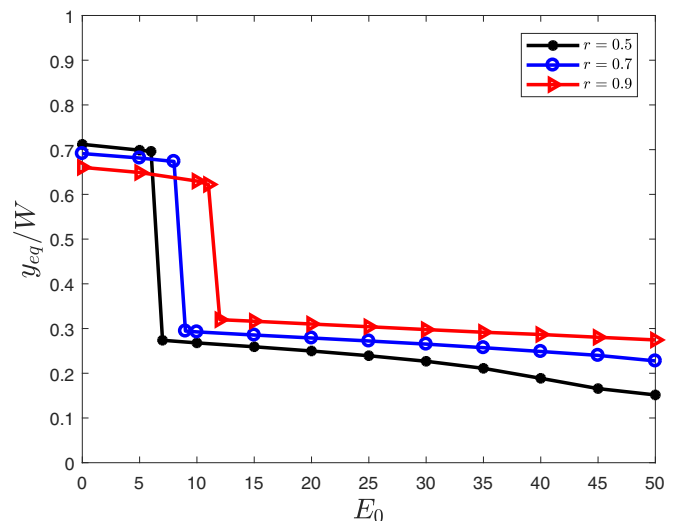


FIG. 10. The lateral equilibrium positions of the charged particle with different sizes.

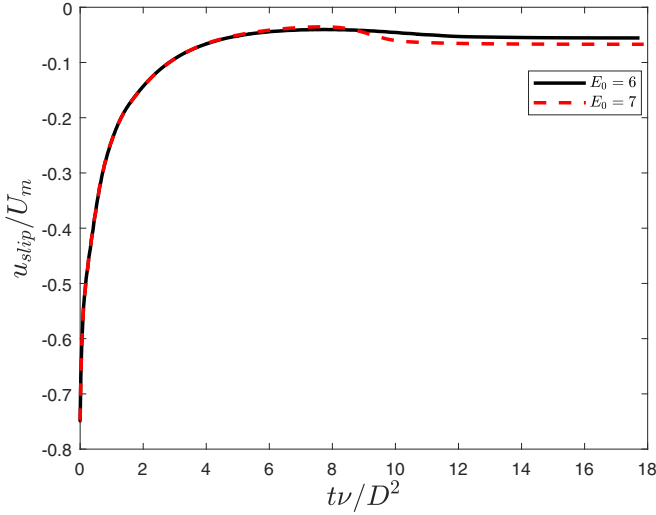


FIG. 11. The evolutions of the slip velocity at $E_0 = 6$ and $E_0 = 7$.

but when particle is far away from the wall, the wall effect would be reduced significantly.

Second, we focused on the effect of the inertial lift related to shear slip. It is known that the shear slip create a slip velocity (u_{slip}) which is the deference between the particle and the fluid velocities ($u_{slip} = u_p - u$). For a particle in the Poiseuille flow, if the slip velocity is positive, the particle leads the fluid, and the inertial lift force push the particle to the wall. However, if the slip velocity is negative, the particle lags the fluid, and the inertial lift force pushes the particle to the centerline [7]. As shown in Fig. 11, the slip velocities at $E_0 = 6$ and $E_0 = 7$ are both negative, and thus the role of the inertial lift force is to push the particle to the centerline.

Third, we considered the effect of the lift due to particle rotation. Figure 12 shows the evolution of the angular velocity of the particle in time for the cases of $E_0 = 6$ and $E_0 = 7$. From this figure, it can be seen that the angular velocity of particle is always positive at $E_0 = 6$, but for the case of

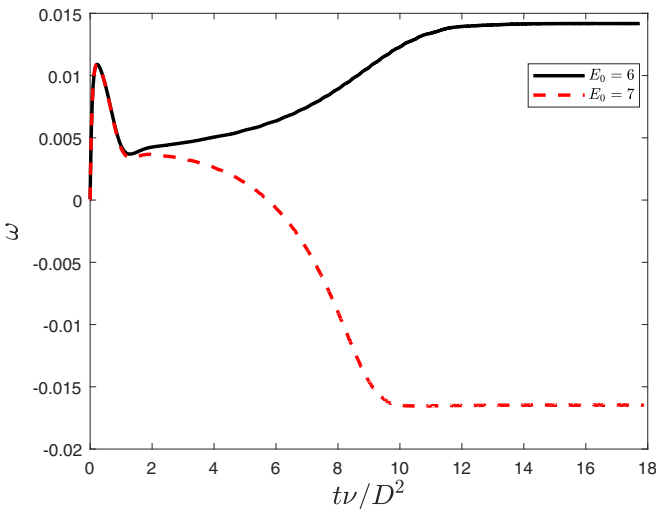


FIG. 12. The evolutions of the angular velocity of the particle at $E_0 = 6$ and $E_0 = 7$.

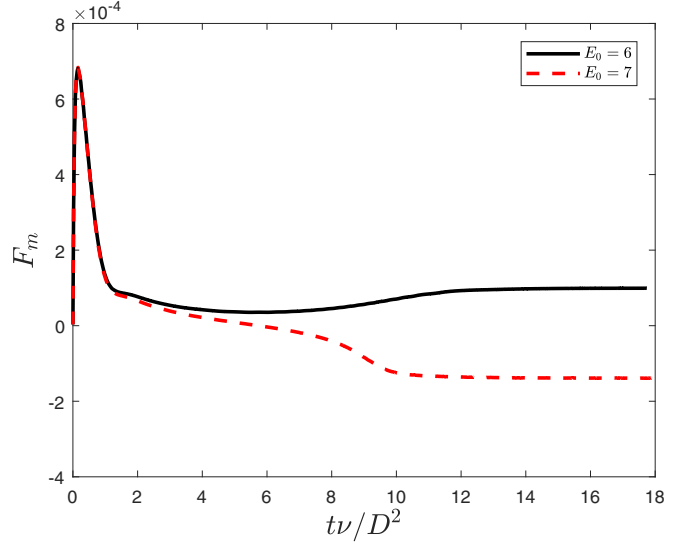


FIG. 13. The evolutions of the Magnus force on the particle at $E_0 = 6$ and $E_0 = 7$.

$E_0 = 7$, it changes from the positive value to the negative value with the time increases. Since the rotation of the particle can drive the surrounding fluid to rotate, the fluid velocity on one side of the particle increases and simultaneously the fluid velocity on the other side decreases. According to Bernoulli's principle, an increase in fluid velocity will result in a decrease in pressure, and a decrease in fluid velocity will result in an increase in pressure, which will lead to a pressure difference in the lateral direction of the rotating particle and form a Magnus force perpendicular to the direction of motion of the particle. The Magnus force is expressed as [32]

$$F_m = \frac{1}{2} \pi \rho D^2 (u - u_p) \omega, \quad (45)$$

which indicates that the direction of the Magnus force is dependent on the angular velocity and the relative velocity of the fluid and particle. When the particle lags the fluid,

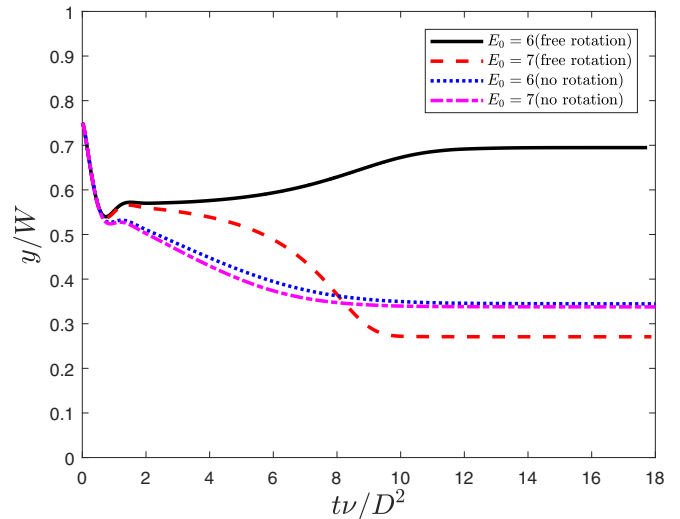


FIG. 14. The migration of freely rotating and nonrotating particles at $E_0 = 6$ and $E_0 = 7$.

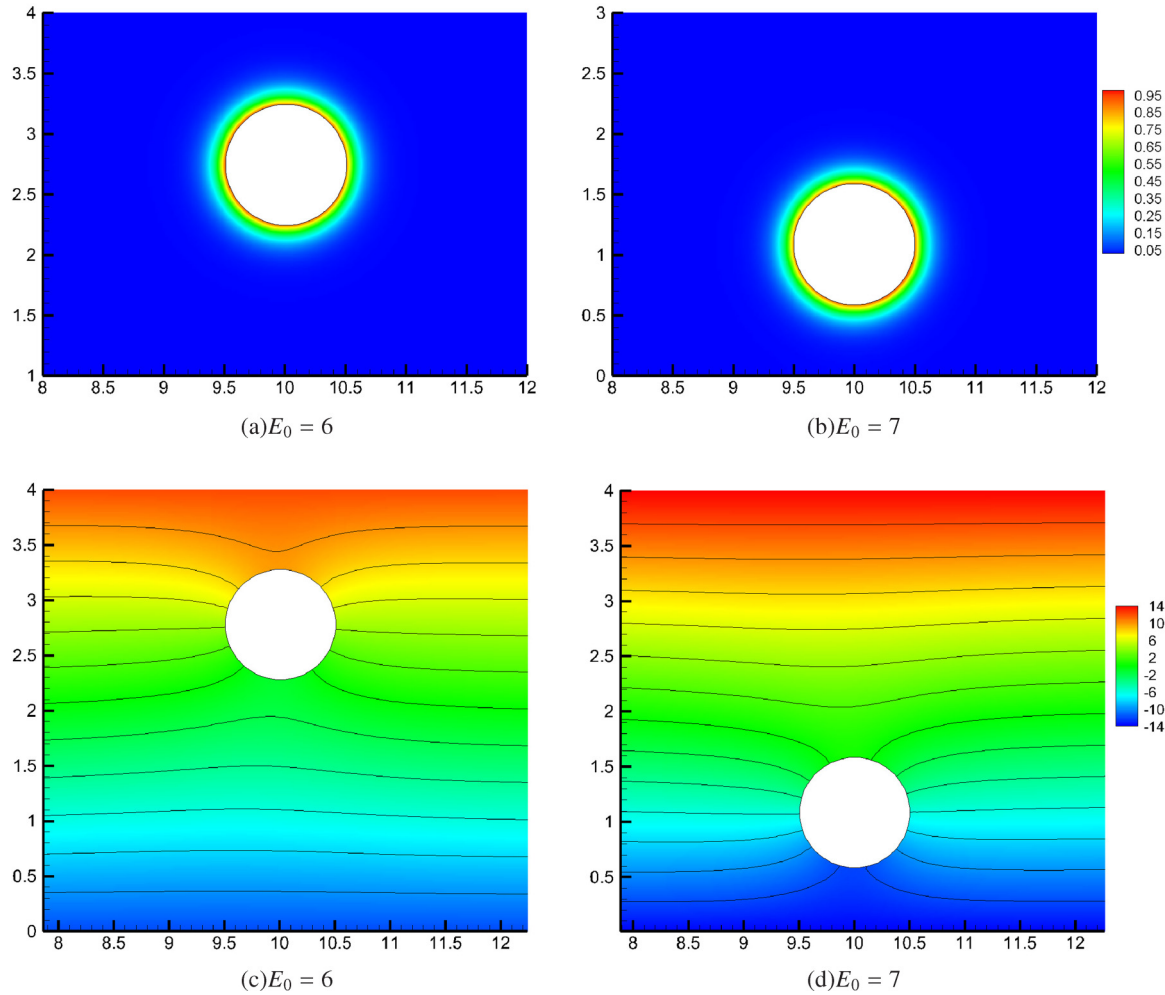


FIG. 15. Internal and external electric potential fields around the particle [(a) and (b) internal electric potential fields, (c) and (d) external electric potential fields].

the direction of the Magnus force is upward if the angular is positive; otherwise the direction of the Magnus force is

downward. As shown in Fig. 13, the Magnus force is always upward at $E_0 = 6$, but with the increase of time, it changes from upward to downward at $E_0 = 7$. In order to better explain the effect of the rotation, we also performed some simulations where the particle is not allowed to rotate. As we can see from Fig. 14, the particle without rotating has a lower equilibrium position at $E_0 = 6$, which means that the lift due to the particle rotation plays a crucial contribution in the transition of the equilibrium position.

Fourth, the effect of a lift due to the curvature of the undisturbed velocity profile is analyzed. For the case of $E_0 = 6$, the velocity of the particle at the steady state is $0.7928U_m$, while the undisturbed fluid velocity is $0.8483U_m$ at the center

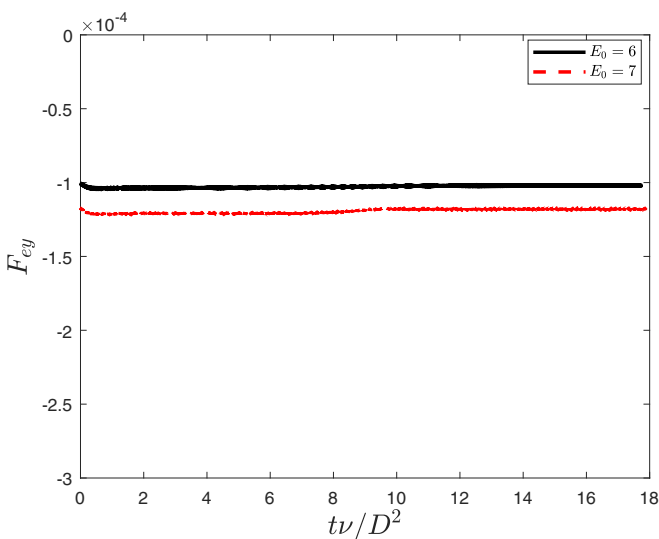


FIG. 16. The evolutions of the electric force on the particle at $E_0 = 6$ and $E_0 = 7$.

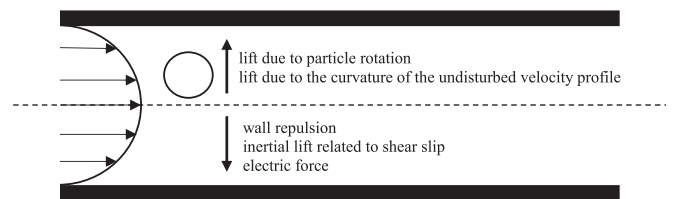


FIG. 17. The mechanisms for the lateral migration of the charged particle in the Poiseuille flow.

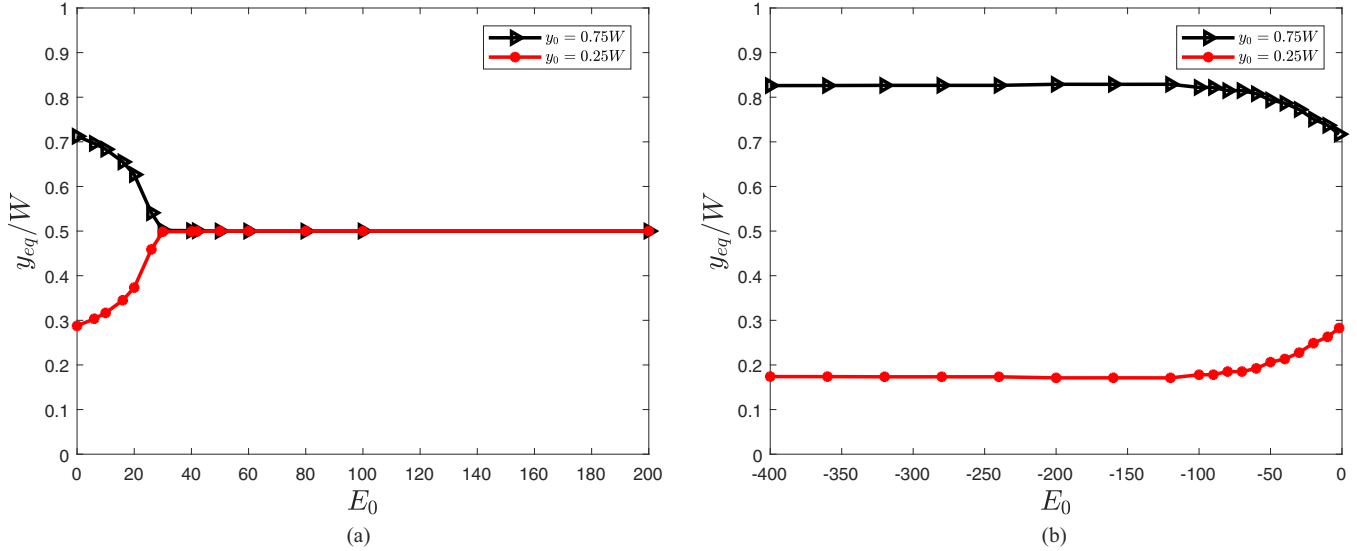


FIG. 18. Lateral equilibrium position of the particle under different values of electric field intensity.

of the particle; the velocity is $0.9805U_m$ at its lower tip which is larger than $0.591U_m$ at the upper tip. This shows that the curvature creates a higher velocity of the fluid relative to the particle on the upper side, which causes a low pressure on the upper side of the particle. In this case, the particle would be pushed away from the centerline. For the case with $E_0 = 7$, the situation is opposite when the equilibrium position of the particle is below the centerline. The velocity of the particle is $0.7227U_m$, and the undisturbed fluid velocity is $0.7898U_m$ at the center of the particle. However, the velocity is $0.4981U_m$ at its lower tip, which is smaller than $0.9565U_m$ at the upper tip. It is also clear that the curvature creates a higher velocity of the fluid relative to the particle on the upper side, which causes a low pressure on the upper side of the particle. Thus, the particle would moves toward the centerline.

The last mechanism of the lateral migration of the charged particle in the Poiseuille flow is the lift force due to the electric field. It should be noted that there is a thin double electric layer around the particle, and the electric charges in the electric double layer move under the effect of the electric force, thereby driving the movement of the surrounding fluid. The electric force acting on the particle leads the particle to move against the surrounding liquid. We presented the internal and external electric potential fields around the particle at $E_0 = 6$ and $E_0 = 7$ in Fig. 15. From this figure, one can find that there is no obvious difference between internal electric potential fields at $E_0 = 6$ and $E_0 = 7$, but the external electric potential fields show a great difference. We also plotted the electric force caused by the external potential field in Fig. 16, and the results show that the particle at $E_0 = 7$ is subjected to a stronger downward electric force than that at $E_0 = 6$. Therefore, the lift due to the electric field is also crucial to the transition of the equilibrium position.

In summary, the equilibrium position of the charged particle in the Poiseuille flow is determined by five competing mechanisms. As illustrated in Fig. 17, for the particle above the centerline, two of them (the lift due to particle rotation, the lift due to the curvature of the undisturbed velocity profile) are upward, while three of them (the wall repulsion due to

lubrication, the inertial lift related to shear slip and the electric force) are downward. For the case of $E_0 = 6$, the downward lift cannot conquer the upward lift, and hence the equilibrium position is above the centerline. For the case of $E_0 = 7$, however, the downward lift can dominate over the upward lift due to the increase of the electric force, which causes the particle to reach a lower equilibrium position.

C. The charged particle motion under a horizontal external electric field

We continued to investigate the effect of the horizontal external electric field on the lateral migration of the charged particle. The electric potential on the particle surface is $\varphi_p = -1.0$, and only two different initial positions $y_0 = 0.75W$ and $0.25W$ are considered. The other parameters are the same as those in the previous part. We carried out some numerical simulations of the particle migration under different values

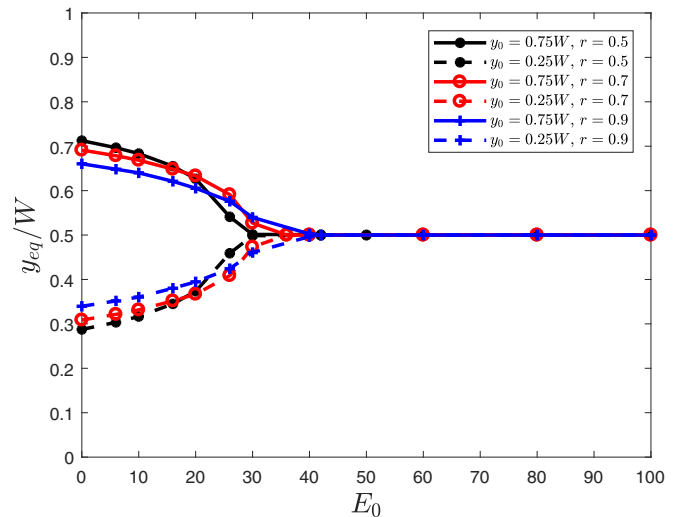


FIG. 19. Lateral equilibrium position of the particle under different particle sizes.

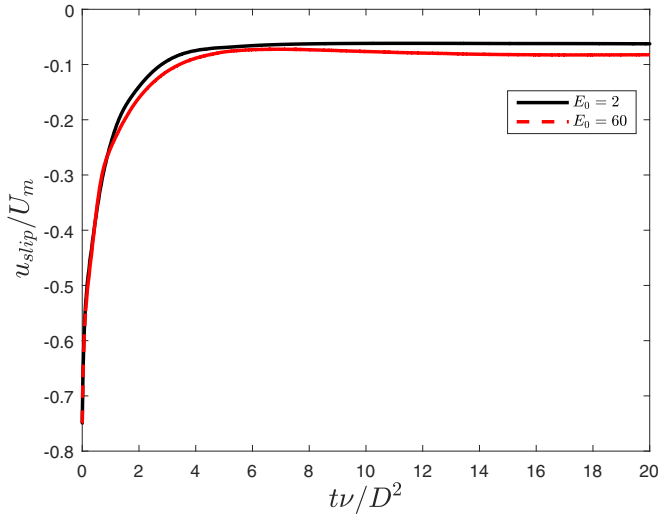


FIG. 20. The evolutions of the slip velocity of the charged particle.

of the electric field intensity (E_0), and presented the results in Fig. 18. As shown in this figure, the equilibrium position of the charged particle is related to the initial position when E_0 is small. The equilibrium position would remain above the centerline if the position of the particle is initially located above the centerline, and vice versa. However, we would like to point out that when E_0 is positive [see Fig. 18(a)], the particle's equilibrium position gradually approaches the centerline with the increase of E_0 . If E_0 is large enough, the equilibrium position of the particle is stable at the centerline, and does not change with the electric field intensity. From the above discussion, it is clear that there is a critical electric field intensity E_c , beyond which the equilibrium position would be only at the centerline. Moreover, it is also found that for two cases with initial positions $y_0 = 0.75W$ and $0.25W$, the equilibrium position of the charged particle is symmetric about the centerline. It indicates that the position of the particle can be

controlled by applying the horizontal external electric field. On the other hand, when E_0 is negative [see Fig. 18(b)], the equilibrium position of the particle is stable at the position of $0.82W$ or $0.18W$ if the magnitude of E_0 is large enough. We note that these above phenomena are qualitatively consistent with the theoretical analysis in the previous study [33].

Figure 19 shows the effect of the particle size on the equilibrium position. It can be seen from this figure that when E_0 is small, the equilibrium position approaches to the centerline as the particle size increases, and the critical electric field intensity E_c increases with the increase of the particle size.

Here it should be noted that unlike in the above discussion, the electric force plays a similar role as the inertial lift related to shear slip. To see this more clearly, we presented the evolutions of the slip velocity in time in Fig. 20 where $E_0 = 2$ and $E_0 = 60$. From this figure, one can observe that a larger electric field intensity results in a larger slip velocity which leads to an increase of the inertial lift. This inertial lift further pushes the particle to the centerline. In addition, we also plotted the evolutions of the angular velocity and the Magnus force at $E_0 = 2$ and $E_0 = 60$ in Fig. 21. As seen from this figure, the angular velocity decreases with the increase of E_0 , which results in a decrease in the Magnus force due to particle rotation, and the particle is pushed to the centerline. We now focused on the effect of the lift due to the curvature of the undisturbed velocity profile. For the case $E_0 = 2$, the velocity of the particle at the steady state is $0.7675U_m$, and the undisturbed fluid velocities at the lower and upper tips are $0.9742U_m$ and $0.5637U_m$. This illustrates that the curvature creates a higher velocity of the fluid relative to the particle on the upper side which causes a low pressure on the upper side of the particle and pushes the particle away from the centerline. When the particle is stabilized at the centerline, it is no longer subjected to lateral forces. Therefore, the equilibrium position of the charged particle in the Poiseuille flow under the influence of the horizontal external electric field is determined by four different mechanisms, as shown in Fig. 22. Actually, as the external electric field intensity increases, the

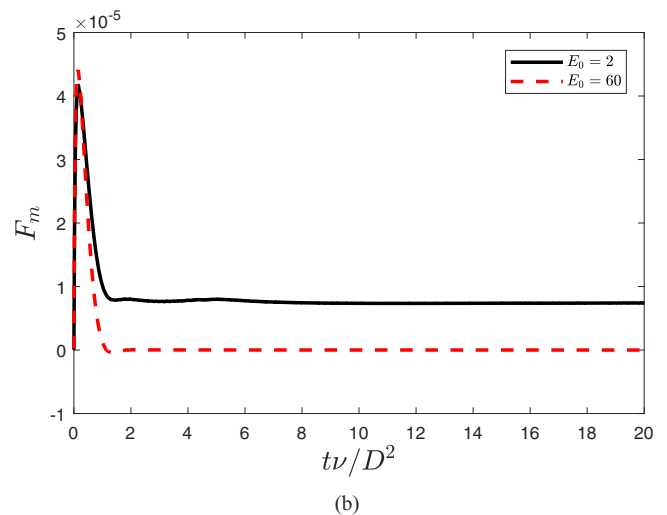
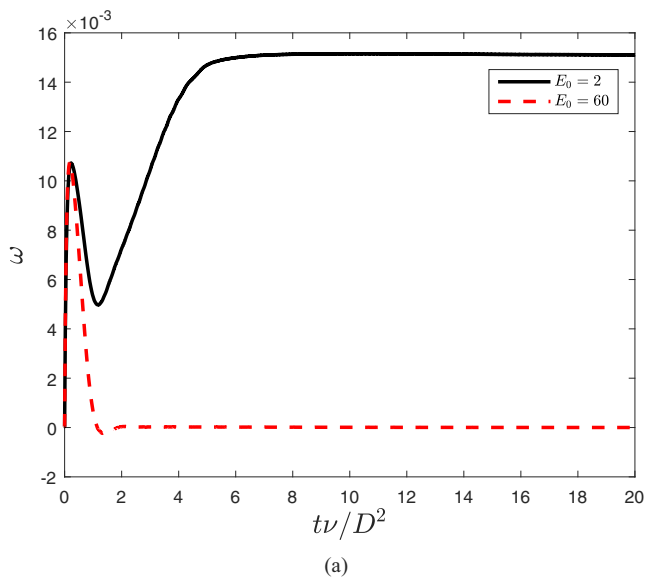


FIG. 21. The evolutions of the angular velocity (a) and Magnus force (b) of the charged particle.

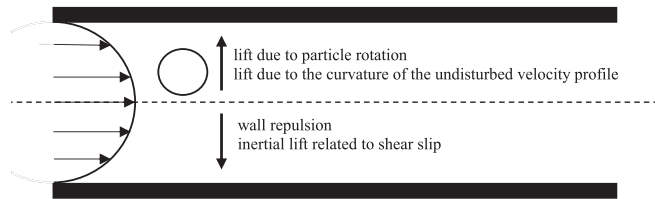


FIG. 22. The mechanisms for the lateral migration of the charged particle in the Poiseuille flow.

wall repulsion and the inertial lift related to shear slip would become strong enough to balance the lifts due to particle rotation and curvature of the undisturbed velocity profile once the particle is at the equilibrium position ($y_{eq} = 0.5W$).

VI. CONCLUSIONS

In this paper, a triple-distribution-function DI-LBM is proposed for the transport of a charged particle in the Poiseuille flow, and a detailed study on the effects of intensity and direction of the electric field, the initial position and the particle size on the lateral migration of the particle in the Poiseuille flow is conducted. The numerical results demonstrate that the external electric field has a significant influence on the lateral equilibrium position of charged particle. When a vertical external electric field is considered, the equilibrium position of particle is dependent on the initial position for a small electric field intensity, but insensitive to the initial position when the electric field intensity is large enough. It is also found that

there is a critical value of electric field intensity that causes an abrupt change of the equilibrium position from above the centerline to below the centerline. These phenomena are determined by the competition among different mechanisms, i.e., the wall repulsion due to lubrication, the inertial lift related to shear slip, the lifts due to particle rotation and the curvature of the undisturbed velocity profile, and the electric force.

On the other hand, when a horizontal external electric field with a small intensity is adopted, the equilibrium position remains above the centerline when the initial position is above the centerline, and vice versa. However, when the electric field intensity is larger than a critical value, the equilibrium position would be at the centerline and independent of the initial position and the electric field intensity. It should be noted that these interesting phenomena are determined by the competition among four different mechanisms, i.e., the wall repulsion due to lubrication, the inertial lift related to shear slip, the lifts due to particle rotation, and the curvature of the undisturbed velocity profile. Finally, it is also found that as the particle size increases, so does the critical value of electric field intensity.

ACKNOWLEDGMENTS

This work was financially supported by the National Natural Science Foundation of China (Grants No. 12072127 and No. 51836003) and the Fundamental Research Funds for the Central Universities, HUST (Grant No. 2021JYCXJJ010).

- [1] G. Segre, *Nature (London)* **189**, 209 (1961).
- [2] D. L. Koch and R. J. Hill, *Annu. Rev. Fluid Mech.* **33**, 619 (2001).
- [3] A. A. S. Bhagat, S. S. Kuntaegowdanahalli, and I. Papautsky, *Microfluid. Nanofluid.* **7**, 217 (2009).
- [4] R. G. Cox and H. Brenners, *Chem. Eng. Sci.* **23**, 147 (1968).
- [5] B. P. Ho and L. G. Leal, *J. Fluid Mech.* **65**, 365 (1974).
- [6] P. Vasseur and R. G. Cox, *J. Fluid Mech.* **78**, 385 (1976).
- [7] J. Feng, H. H. Hu, and D. D. Joseph, *J. Fluid Mech.* **277**, 271 (1994).
- [8] T. Inamuro, K. Maeba, and F. Ogino, *Int. J. Multiphase Flow* **26**, 1981 (2000).
- [9] X. Shao, Z. Yu, and B. Sun, *Phys. Fluids* **20**, 103307 (2008).
- [10] J. Hu and Z. Guo, *Int. J. Heat Mass Transf.* **108**, 2158 (2017).
- [11] C. Ye and D. Li, *Microfluid. Nanofluid.* **1**, 52 (2004).
- [12] S. Bhattacharyya and P. P. Gopmandal, *Colloids Surf. A* **390**, 86 (2011).
- [13] C. Xie, B. Chen, C. Ng, X. Zhou, and J. Wu, *Eur. J. Mech. B Fluids* **49**, 208 (2015).
- [14] N. Tofighi, J. J. Feng, M. Yildiz, and A. Suleman, *Int. J. Multiphase Flow* **135**, 103524 (2021).
- [15] S. Y. Chen and G. D. Doolen, *Annu. Rev. Fluid Mech.* **30**, 329 (1998).
- [16] S. Succi, *The Lattice Boltzmann Equation for Fluid Dynamics and Beyond* (Oxford University Press, Oxford, UK, 2001).
- [17] Z. Guo and C. Shu, *Lattice Boltzmann Method and Its Applications in Engineering* (World Scientific, Singapore, 2013).
- [18] T. Krüger, H. Kusumaatmaja, G. Silva, O. Shardt, A. Kuzmin, and E. M. Viggien, *The Lattice Boltzmann Method: Principles and Practice* (Springer International, Cham, Switzerland, 2017).
- [19] Y. Zhao, G. Pereira, S. Kuang, and B. C. Shi, *Appl. Math. Lett.* **114**, 106926 (2021).
- [20] X. Liu, Z. H. Chai, and B. C. Shi, *Commun. Comput. Phys.* **30**, 1346 (2021).
- [21] A. J. C. Ladd, *J. Fluid Mech.* **271**, 285 (1994).
- [22] A. J. C. Ladd and R. Verberg, *J. Stat. Phys.* **104**, 1191 (2001).
- [23] Z. G. Feng and E. E. Michaelides, *J. Comput. Phys.* **195**, 602 (2004).
- [24] J. Liu, C. H. Huang, Z. H. Chai, and B. C. Shi, *Comput. Fluids* **233**, 105240 (2022).
- [25] Z. H. Chai and B. C. Shi, *Appl. Math. Model.* **32**, 2050 (2008).
- [26] J. Liu, Z. H. Chai, and B. C. Shi, *Int. J. Mod. Phys. C* **31**, 2050043 (2020).
- [27] Y. H. Qian, D. d'Humières, and P. Lallemand, *EPL* **17**, 479 (1992).
- [28] Z. Guo, C. Zheng, and B. Shi, *Phys. Rev. E* **65**, 046308 (2002).
- [29] S. Tao, J. J. Hu, and Z. L. Guo, *Comput. Fluids* **133**, 1 (2016).
- [30] R. Trunk, T. Weckerle, N. Hafen, G. Thäter, N. Hermann, and M. J. Krause, *Computation* **9**, 11 (2021).
- [31] H. Liu, S. Qian, and H. H. Bau, *Biophys. J.* **92**, 1164 (2007).
- [32] J. Lin and J. Li, *Int. J. Nonlinear Sci. Numer. Simul.* **5**, 9 (2004).
- [33] A. Choudhary, T. Renganathan, and S. Pushpavanam, *J. Fluid Mech.* **874**, 856 (2019).